

## ISROMAC 2006-057

### IMPACT OF A FILLET ON DIFFUSING VANE ENDWALL FLOW STRUCTURE

*Martin Hoeger,*  
MTU Aero Engines  
Dep. TEAD, Compressor Aero  
D 80995 Munich/ Germany  
Martin.Hoeger@muc.mtu.de

*Ralf Dietmar Baier*  
MTU Aero Engines  
Dep. TEAD, Aerodynamics  
D 80995 Munich/ Germany  
Ralf-D.Baier@muc.mtu.de

*Ralf Müller*  
Dresden University of Technology  
Institute of Fluidmechanics  
D 01062 Dresden/ Germany  
Mueller@tus.mw.tu-dresden.de

*Martin Engber*  
MTU Aero Engines  
Dep. TETV, Compressor Technology  
D 80995 Munich/ Germany  
Martin.Engber@muc.mtu.de

#### ABSTRACT

To further extent compressors loading limits, basic experiments were conducted on a compressor cascade at the Dresden University of Technology. Engine-like loading levels and high incidences are investigated. The results for a datum blade and two fillet configurations with relative radii of 8% and 16% chord are compared with simulations. Numerical studies with different inlet boundary layer twist and displacement thickness were made.

Careful analysis of the simulations allows an improved understanding of corner stall: while the datum blade stalled early for highly twisted inlet boundary layers, the fillet configurations allowed for higher incidences at the endwall. As a result, high incidence, counter-swirling flow entered the blade passage, reduced the secondary cross-flow and made higher loading levels and reduced losses possible

#### INTRODUCTION

In the literature a large number of investigations on stall phenomena in the rotor passages of axial compressors exist, see [1]. An excellent visualization of the flow structure at stall inception is given in [2]. However, it is often overlooked that the surge margin of a compressor is also influenced by the stator hub and tip regions. Vane geometry, leading edge shape and the

presence of a fillet can have a considerable impact on the stability of the compression system.

To control endwall flow and enhance stability several measures exist. For an industry gas turbine with high hub loading Stringham et al. [3] reported a 2% efficiency improvement from removing corner stall by an advanced endwall contour. In Hoeger et al. [4] a comparison of several types of endwall contours is made and the impact on secondary flow structure is investigated. To further reduce endwall losses, a bulb configurations was first introduced by Dresden University in turbines blades [5]. An advanced leading edge modification, which combines a fillet and a bulb is presented by Shih, and Lin in [6]. Experimental results for the present cascade with a bulb modification, see Müller et al. [7], clearly demonstrate a 30% loss reduction potential in the endwall region. The presence of a fillet was demonstrated by DeBruge [8] to reduce the magnitude of the boundary layer in the endwall region. Curlett and Breugelmanns [9], [10] showed a fillet at high incidences to favorably influence the losses. In [11] similar results are reported for the present cascade and a so-called fillet vortex was visualized on the basis of the simulations. This fillet vortex turned in the opposite direction to the horse-shoe vortex typically found in front of a blunt body placed on a wall. Neither a stagnation point nor a horse-shoe vortex were found in [11] for a large fillet.

In an early reference Klein [12] demonstrates how counter-swirl from boundary layer twist for a turbine amplifies secondary flow and increases endwall losses. In [12] it is stated that for axial compressors at design conditions there is little impact of the endwall boundary layer state on the blade performance. In this paper the impact of a twisted inlet boundary layer at off design conditions is investigated. A fillet is demonstrated to be an effective measure to remove corner stall, to enhance stability and to install higher loading levels.

## NOMENCLATURE

$\alpha, \alpha_l$	flow angle, see Fig.1 page 3
$c$	chord length
$\delta_1$	boundary layer displacement thickness
$H$	$H$ half passage height of 2D cascade, $H=150\text{mm}$
$H_{12}$	incompressible boundary layer shape parameter
$Ma$	Mach number
$v$	velocity, in direction of 2D flow at midspan
$x, y, z$	co-ordinate directions, axial-, circumferential- and spanwise direction, see Fig. 1
$\zeta_i(z)$	circumf. mass av. loss coeff., $i=1,2$ , see eq. (1) page 3
$\zeta_{ew,0}$	Zeta,ew,0: total net endwall loss coeff., normalized for an aspect ratio $2H/c=1$ , see eq. (2), page 3
$ax$	axially oriented
$ew$	endwall (hub)
$ms$	mid span
$sw$	b.l. profiles with swirl twist, e.g. $sw10 = 10\text{deg}$ twist
1	inlet reference planes $x/cax = -0.25$ , see Fig. 1
2	exit reference planes $x/cax = 1.5$ , see Fig. 1

exit guide vanes, generate strong secondary flows. The resulting so-called endwall boundary layers have to be controlled by advanced 3D blade design strategies. For code validation issues and to investigate the improvement potential from leading edge optimization, 2D cascade tests have been analyzed [11], [13], [14]. To transfer this knowledge into improved engine designs, the impact of distorted inlet boundary layer profiles on corner stall is investigated on the basis of simulations.

## CASCADE DESIGN

A large scale low speed cascade wind tunnel was chosen to best resolve secondary flow from large dimensions.

### Cascade Geometry

**Cascade Parameters** The cascade design was made with emphasis on endwall flow. In the hub region an engine like loading level with diffusion factors close to 0.5 is found, while in the mid section moderate loading levels with diffusion factors around 0.375 occur, see table 1 for main geometric and aerodynamic parameters. Further details on geometry are found in Fig. 1.

### Engine Relevance

2D cascade testing on one side has the advantage of allowing to investigate most precisely certain aspects of the flow. On the other hand important flow features like blade row interaction, rotation, work input, unsteadiness and endwall boundary layer shear are not included and (although their impact on the flow field often is known to be non-linear) they have to be taken into account by the engine designer. Only by that, knowledge gained from 2D cascade investigations may be used to improve engine designs.

**Endwall Modifications** In this paper investigations for 2 fillets and a datum configuration are presented. While the fillet with a constant 8mm radius ( $r/c = 8\%$ ) may cover the upper range of what is found for compressor blades and vanes in engine, a large fillet with 16mm ( $r/c = 16\%$ ) is introduced to work out fillet impact on flow more precisely and to cover strut and turbine exit guide vane cases too.

### Inlet Conditions

**Inlet Boundary Layer:** Inlet boundary layer parameters from experiment and those used in the simulations are given in Fig. 2. An average inlet boundary layer thickness of  $\delta_1 = 3.8\text{mm}$  is found in experiment, which translates into an inlet blockage of about  $\delta_1/H = 2.5\%$ . Depending on the choice of the edge of the boundary layer an upper and a lower value may be deduced from the measurements, see 2 lines in Fig. 2.

**Swirl Angle:** To link the basic cascade investigations with the flow conditions in engine, multi-stage predictions for several compressor vanes are investigated. Moderately loaded compressor vanes (4 compressors, first 3 stages, diffusion factors around 0.35 to 0.45, aspect ratios between 1 and 2.5, vane design both build and cantilevered) have been analyzed to

Compressor cascade V63			
chord length	$c$	0.100	M
pitch/ chord ratio	$s/c$	0.62	-
rel. max. thickness	$t/c$	5.5	-
cascade aspect ratio	$2H/c$	3.0	-
flow turning $\Delta\alpha$ (design incidence $i=2$ )		21	deg
inlet Mach number, simulations $Ma_1$		0.24	-
inlet boundary layer displacement thckn.		0.004	m
Reynolds number $Re_c$		$5.4 \cdot 10^5$	-
S1 Diffusion factors endwall/ mid section		0.5/ 0.375	-
Inlet flow angle ( incidence $i=2$ )		36	deg

Table 1: Cascade geometric and aerodynamic parameters

## BACKGROUND AND MOTIVATION

With the inclusion of fillets, cavities and other real geometry effects in a 3D Navier-Stokes based design system, there is a need for a data base to validate turbulence models and to investigate the impact of the grid geometry on the resolution of the flow field.

Furthermore high loading levels found for today's low aspect ratio compressor designs, for struts as well as for turbine

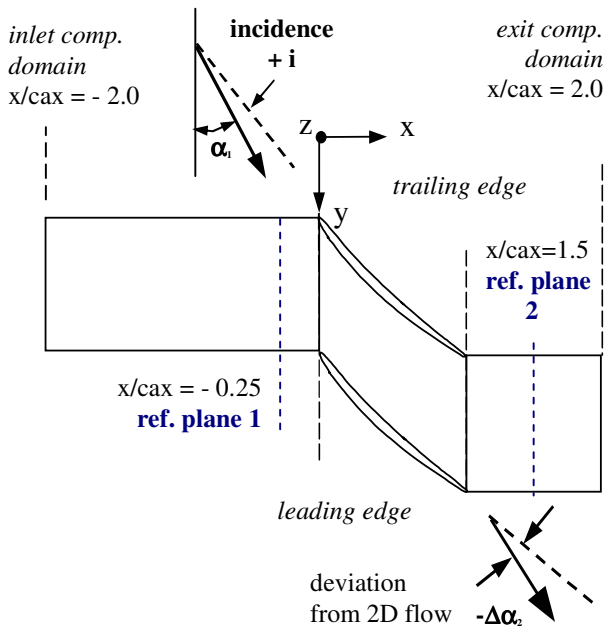


Fig. 1: Cascade geometry, reference planes and flow angle definitions

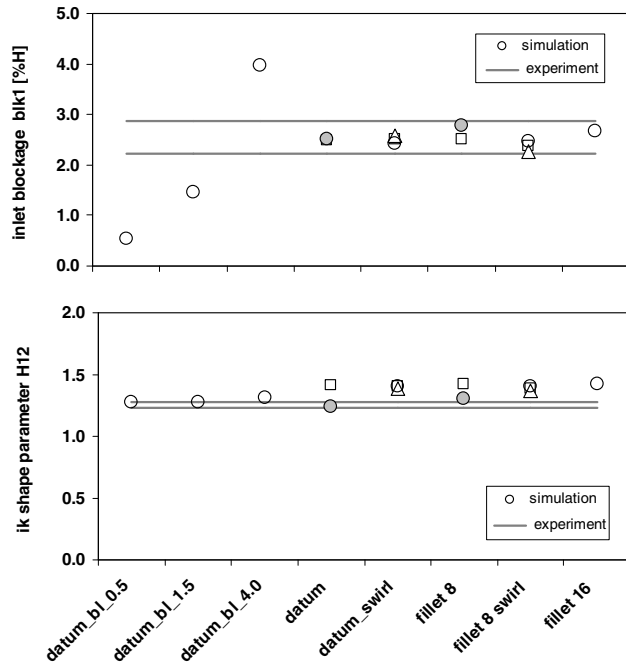


Fig. 2 Inlet boundary layer shape parameter  $H_{12}$  (top) and endwall blockage  $blk1$  (bottom)

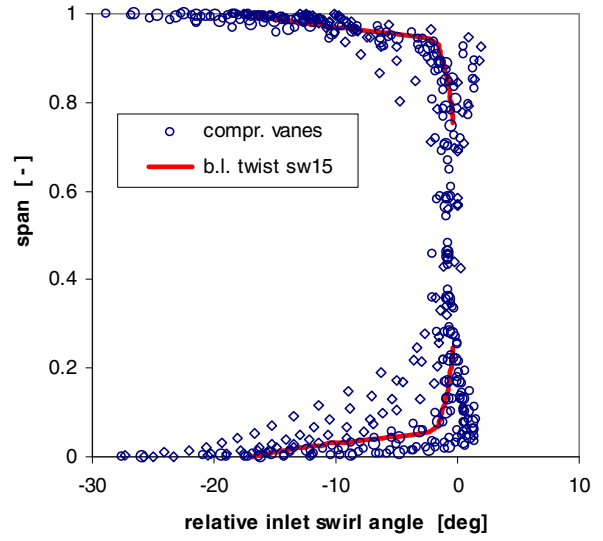


Fig. 3: Compressor vane inlet swirl profiles and swirl modifications used for cascade simulations

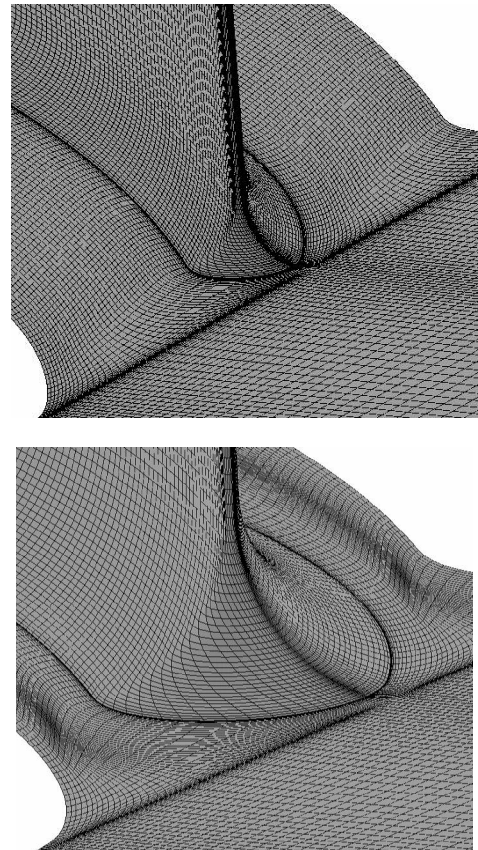


Fig. 4 Grid details for fillet 8 (top) and fillet 16 (bottom) configurations

approximately define a representative average inlet boundary layer shear. The results given in Fig. 3 show a wide range of vane inlet swirl. An average swirl increase of about 15 deg is found at the endwalls.

## NUMERICAL SIMULATIONS

The 3D Navier-Stokes RANS code TRACE\_S was used, a joint development of DLR and MTU, see Fritsch et al. [15]. Simulations performed with a higher order unsteady version TRACE\_U (applied in the steady mode) ensured the results not to be compromised by any shortfall in modeling. Only the 2 deg incidence case where corner stall starts to develop is discussed here. Results for other inlet flow angles not presented in this paper confirm the present investigations.

### 3D Navier-Stokes Solver

An implicit steady version of TRACE\_S and a  $k-\omega$  low Reynolds turbulence model, without transition was used for the cascade blade profiles. About 5 % higher profile losses are found from turbulent simulations. However, any shift in transition point location would have prevented a precise prediction of secondary losses, see chapter on evaluation of results. Wall functions are applied only at the endwalls. Additional simulations with low Reynolds model for all surfaces (here results are slightly closer to experiment), coarser grids and other turbulence models, e.g. a  $k-\epsilon$  model, confirm the present results.

**Simulations:** Specifying static pressure at the exit, the half cascade section was used with a symmetry plane at the mid section. The inlet/ exit of the computational domain is located 2 axial chord length up- and downstream of the cascade inlet plane. Swirl distortion profiles with 10, 20 and 30 deg deviation are described at the inlet of the computational domain to yield a maximum swirl increases in reference plane 1 of about 5, 10 and 15 deg. All other simulations have been run with constant inlet swirl.

Simulations were performed within a *LINUX* cluster using 2 processors with about 50 CPU hours/ 16000 iteration to achieve convergence. Only 2 simulations have been performed for the experimental inlet Mach number  $Ma_1=0.191$  to most accurately compare with measurements. Because convergence proofed to be lengthy for low inlet Mach numbers  $Ma < 0.2$ , all other simulation were run at a slightly higher Mach number level of 0.235. A comparison with experimental values is made in Tab. 2. From a loss correction estimate assuming the relation loss coeff.  $\sim Re^{-0.2}$  (*Wassel's* correlation), a small impact of Reynolds number on loss level of about 3.7% is found.

	Mach No	Reynolds No.	fact. sim/exp
Experiment	0.191	$4.5 \cdot 10^5$	-
Simulation	0.235	$5.4 \cdot 10^5$	1.037

Table 2: Mach and Reynolds numbers for simulation and experiment,

## Grid generation

A standard H-O grid combination is used. Average  $y^+$  values at the profile are between 1 and 2. Fig 4 shows details of the grid for the 2 fillet configurations. Only standard grid topology is used in this paper. For the large fillet configuration close to the endwall in fig. 4 distorted grid lines are visible. New grid strategies are currently tested at MTU to enable grids with minimum node numbers and optimum resolution of the flow field.

## Evaluation of results

**Postprocessor** Mass-average values are used to accurately compare with experimental results. Flow visualization was performed with *VISUAL*.

**Definition of Loss Coefficients** Pitchwise mass averaged total pressures  $pt_{i,av}$  for the reference planes  $i = 1$  and  $2$  at the inlet and the exit of the cascades are used. Subtracting profile loss coefficient in the mid section (index *ms*), a net endwall loss coefficient may be defined by

$$\zeta_{ew} = \zeta_2 - \zeta_{inl,bl} - \zeta_{prof} \quad (1)$$

with

$$\zeta_2 = (pt_{1,is} - pt_{2,av}) / (pt_1 - p_1)$$

$$\zeta_{inl,bl} = (pt_{1,is} - pt_{1,av}) / (pt_1 - p_1)$$

$$\zeta_{prof} = (pt_{1,is} - pt_{2,av,ms}) / (pt_1 - p_1).$$

Hereby the local loss coefficients are first mass averaged in spanwise direction before used to evaluate eq. (1). Provided the regions with 3D flow at the endwalls are not extending up to the mid section, a total net endwall loss coefficient may be defined for the whole cascade (both endwalls) normalized for an aspect ratio of  $2H/c = 1$  by:

$$\zeta_{ew,o} = 2\zeta_{ew} \cdot 2H/c \quad (2)$$

Results from eq. (2) may be applied to similar compressor vane designs by simply multiplying the loss coefficient data with the corresponding aspect ratio.

## ANALYSIS OF RESULTS

Only the 2 deg incidence case is discussed. Results for other inlet flow angles support the findings presented in this paper. Measured data used are in good agreement with those from a curve fit for the whole incidence range.

### Comparison Experiment – Simulation

**Datum Configuration:** Measured inlet velocity- and swirl profiles for the datum cascade are compared to simulations for 4 different inlet boundary layer profiles in Fig. 5, left side. Only a small spanwise gradient for the circumferentially averaged inlet swirl angles is found for the experimental data, see Fig. 5, right side. In the exit plane net loss coefficients and exit flow

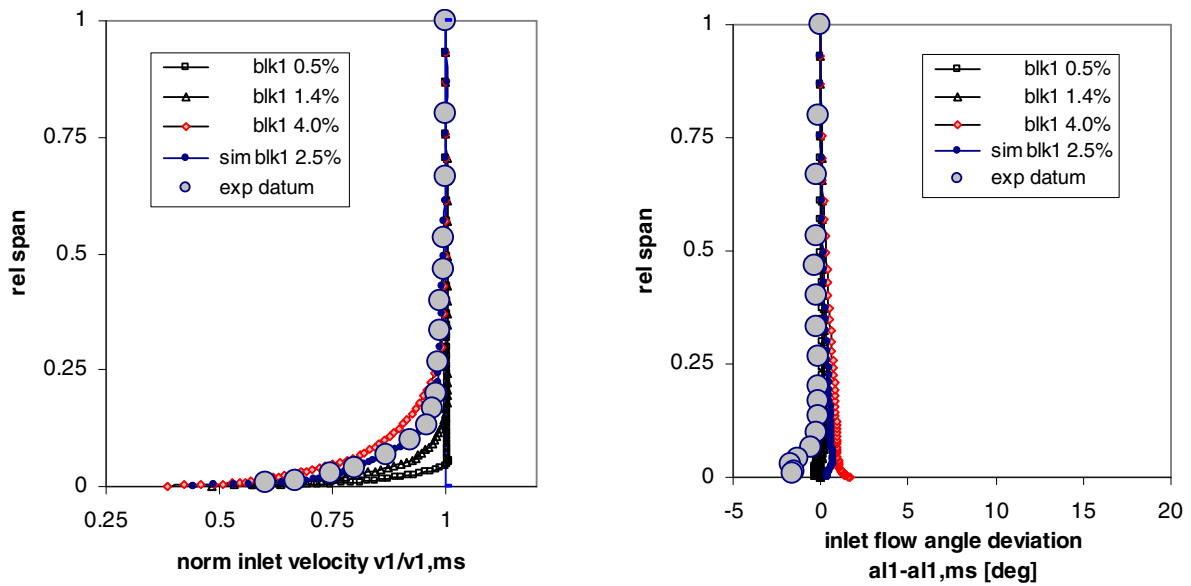


Fig. 5: Inlet conditions, experiment vs simulation with varying inlet boundary layer blockage for datum cascade. Normalized velocity profiles (left side), inlet swirl deviation from 2D flow (right side)

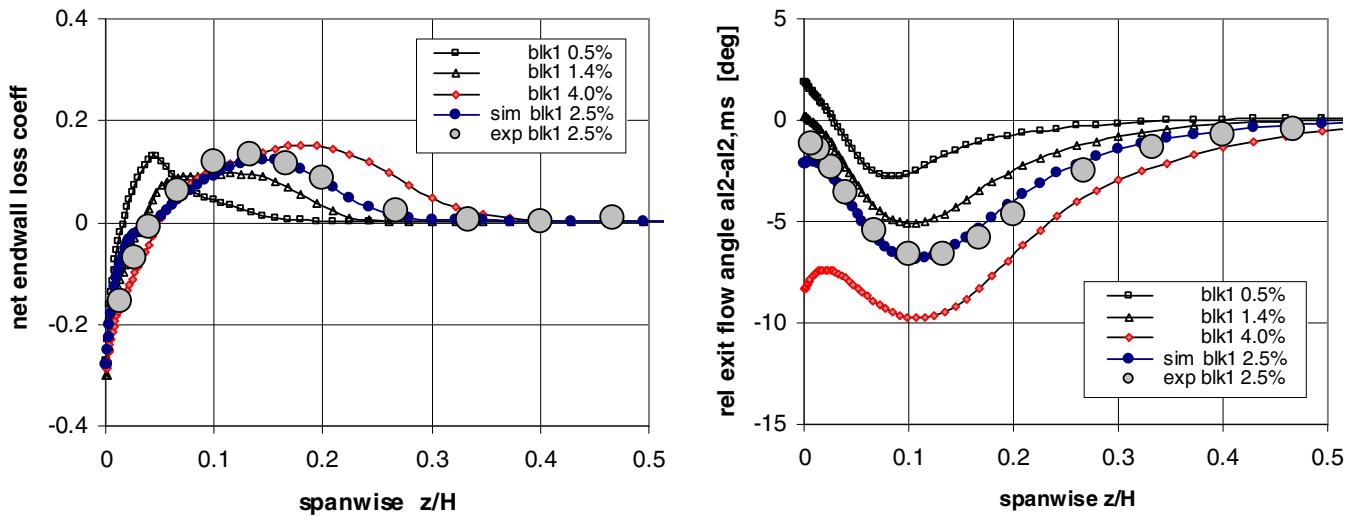


Fig. 6 Comparison of experimental results for net endwall loss coefficient vs simulations with varying inlet boundary layer blockage

Fig. 7 Comparison of experimental results for exit flow angle deviation from 2D flow vs simulations with varying inlet boundary layer blockage

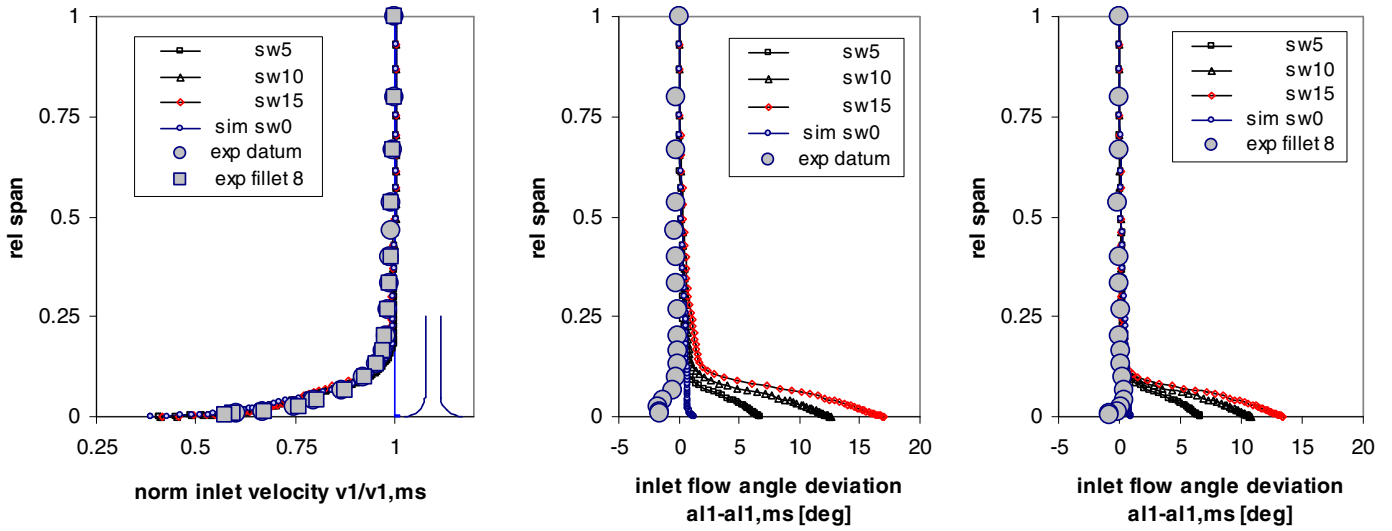


Fig. 8: Inlet conditions experiment vs simulations with twisted inlet swirl profiles.  
 Normalized velocity profiles (left side),  
 inlet swirl twist deviation from 2D flow: datum cascade (mid) and fillet 8mm (right side)

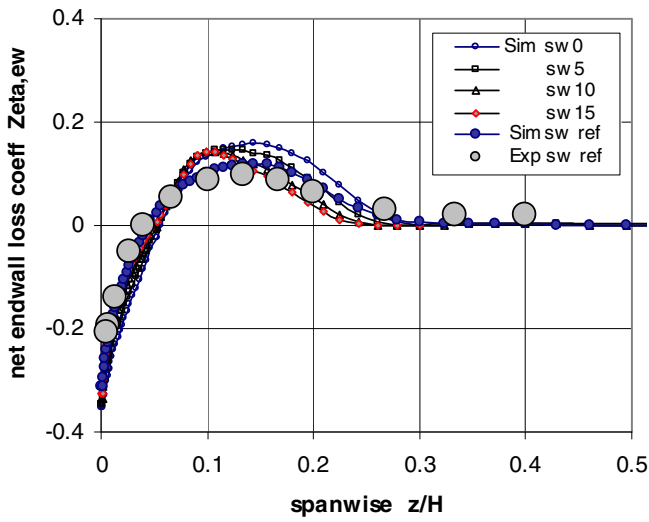


Fig. 9 Fillet 8 configuration. Comparison of experimental results for net endwall loss coefficient vs simulations with varying inlet boundary layer swirl twist, see Fig. 8, right side. For def. loss coeff see eqn. (1)

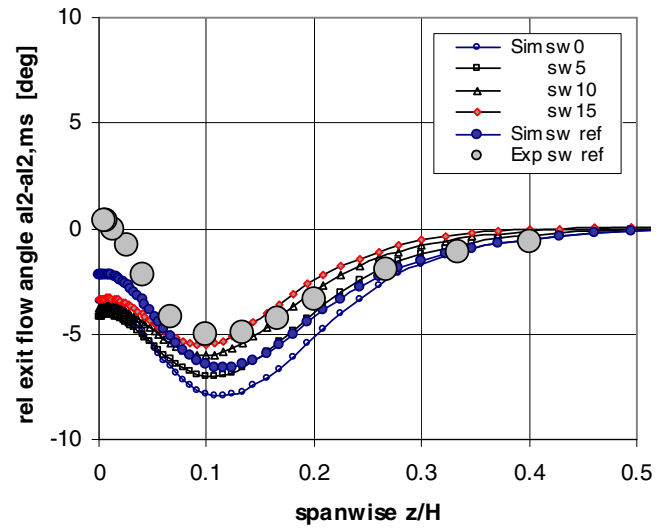


Fig. 10 Fillet 8 configuration. Comparison of experimental results for exit flow angle deviation from 2D flow vs simulations with varying inlet boundary layer swirl twist, see Fig. 8, right side

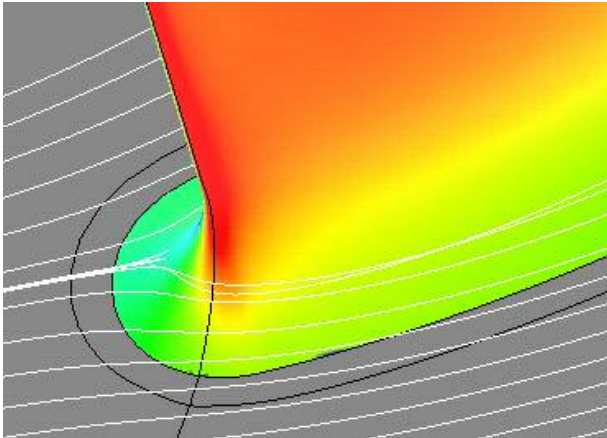


Fig 11: Suction surface isentropic Mach number contours and streamlines close to the endwall for fillet 8 config. at 15 deg inlet boundary layer swirl twist

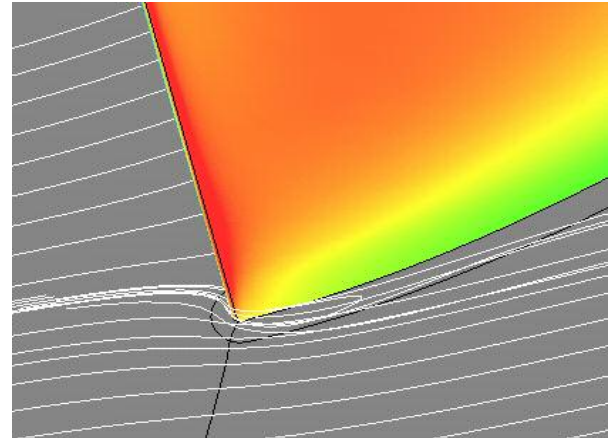


Fig 12: Suction surface isentropic Mach number contours and streamlines close to the endwall for datum cascade at 15 deg inlet boundary layer swirl twist

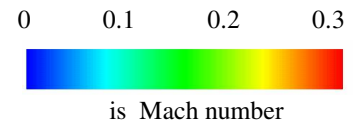
angle deviations from 2D given in Fig. 6 and 7, show good agreement. The secondary flow dependent exit flow angle variation, relative to the 2D flow at the mid section, is predicted with the  $k-\omega$  turbulence model to an accuracy of better than 1 degree. With all relevant secondary flow movements for the datum cascade to be captured, in the following chapter numerical simulations are used to investigate the impact of distorted inlet conditions on endwall flow.

### Fillet 8 Configuration

The calculated net endwall loss coefficients and relative exit flow angles are compared to the experimental results in Fig. 9 and 10. About 2 degrees lower turning is found for the simulations compared to experiment, see full symbols for the simulation with the reference inlet boundary layer profile (which fits to the experiment) as given in Fig. 5. Close to the endwall the fillet is understood not to fulfill any *Kutta*-condition, i.e. for the steady simulations there is no defined exit flow direction like it is known to exist for a thin trailing edge.

Velocity profiles with swirl twist are given in the left part of Fig 8. For an inlet boundary layer profile with nominal inlet blockage of  $blk1 = 2.5\%$  but with a somewhat higher shape parameter  $H_{12}$  swirl distortions have been described at the inlet of the computational domain. In the reference inlet plane about 5, 10 and 15 degrees swirl were found, so that the swirl distortions are referenced  $sw5$ ,  $sw10$  and  $sw15$ , respectively. For a comparison with typical vane inlet swirl distortions see Fig. 3. A pronounced upstream impact of the fillet on the inlet flow angle is found for the higher swirl distortions  $sw10$  and  $sw15$ , see Fig. 8, mid and right side. Regardless the level of swirl distortion entering the cascade, always the same low exit flow angle is found, i.e. the secondary flow movements are balanced by the swirl distortions.

The local net endwall loss coefficients in Fig. 10 show somewhat higher values at nominal swirl  $sw0$ , which



corresponds to the higher underturning and higher cross-flow already found for the exit flow angles Fig. 9. The higher boundary layer swirl reduces the endwall losses and it improves the turning for the fillet, while the datum cascade (radial distributions are not given here) showed increased loss and undertuning for the highest swirl distortions  $sw10$  and  $sw15$ , see chapter on total net loss at the end.

### Mach number distributions from simulation

**Nose Region:** Streamline pattern and surface isentropic Mach numbers for the fillet 8 and the datum cascade with inlet boundary layer swirl distortion  $sw15$  are given in Figs. 11 and 12. A suction peak partly stemming from the swirl distortion in the blade leading edge endwall junction (see red area in Fig. 12) for the datum blade is demonstrated to promote early leading edge stall. Here the fillet, which possesses no stagnation point in the vicinity of the endwall, allows the incoming streamlines to travel smoothly around the nose region.

**Profile Section Mach Number Distributions:** Profile section isentropic Mach number distributions for fillet 8 are compared to the datum cascade in Fig 13 at nominal swirl  $sw0$ . On the pressure surface over-speeds are visible for the fillet 8, while similar Mach number distributions are found in the suction surface leading edge region at all spanwise locations compared to the datum cascade. Towards the trailing edge, at 0.5% and 2.5% span the datum cascade shows an increasing

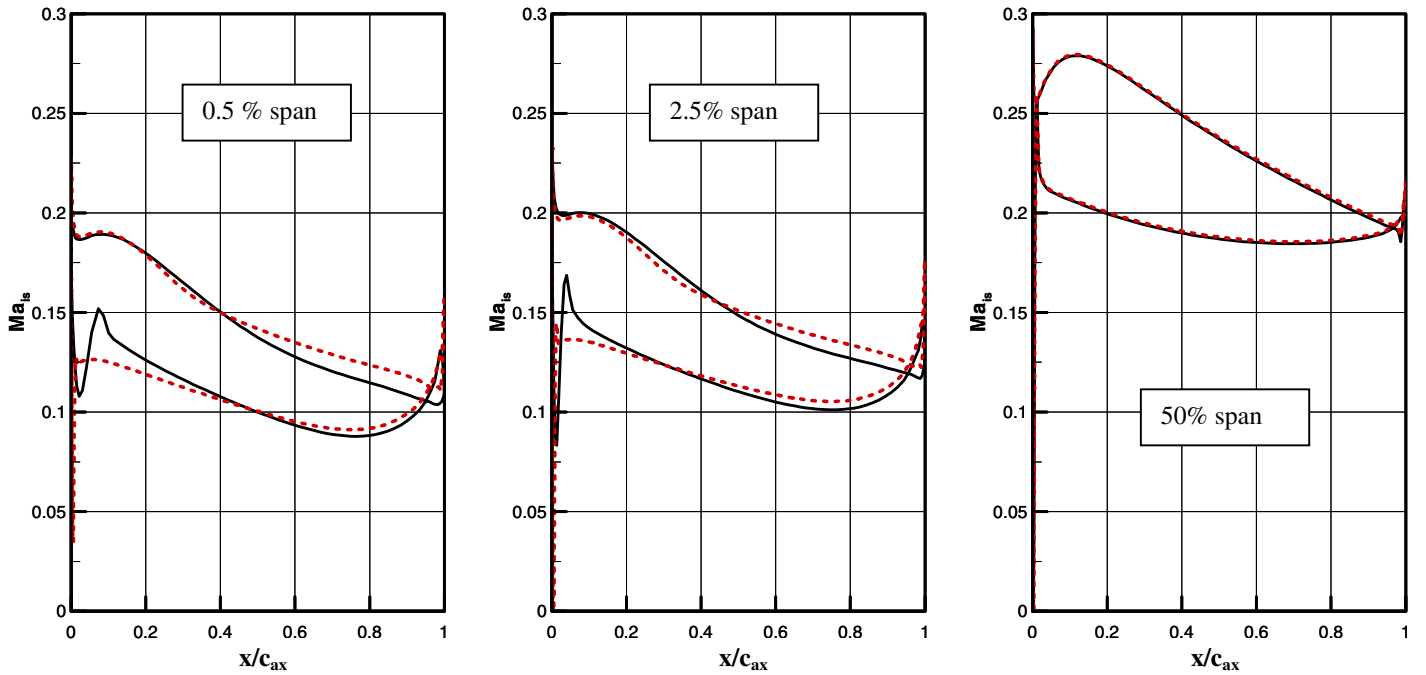


Fig. 13 Comparison of isentropic profile section Mach number distributions at constant inlet swirl. fillet r8 (full line) vs. datum configuration (dashed, red line) at stations near endwall (0.5% span), at half fillet height (2.5% span) and in 2D flow (50%span).

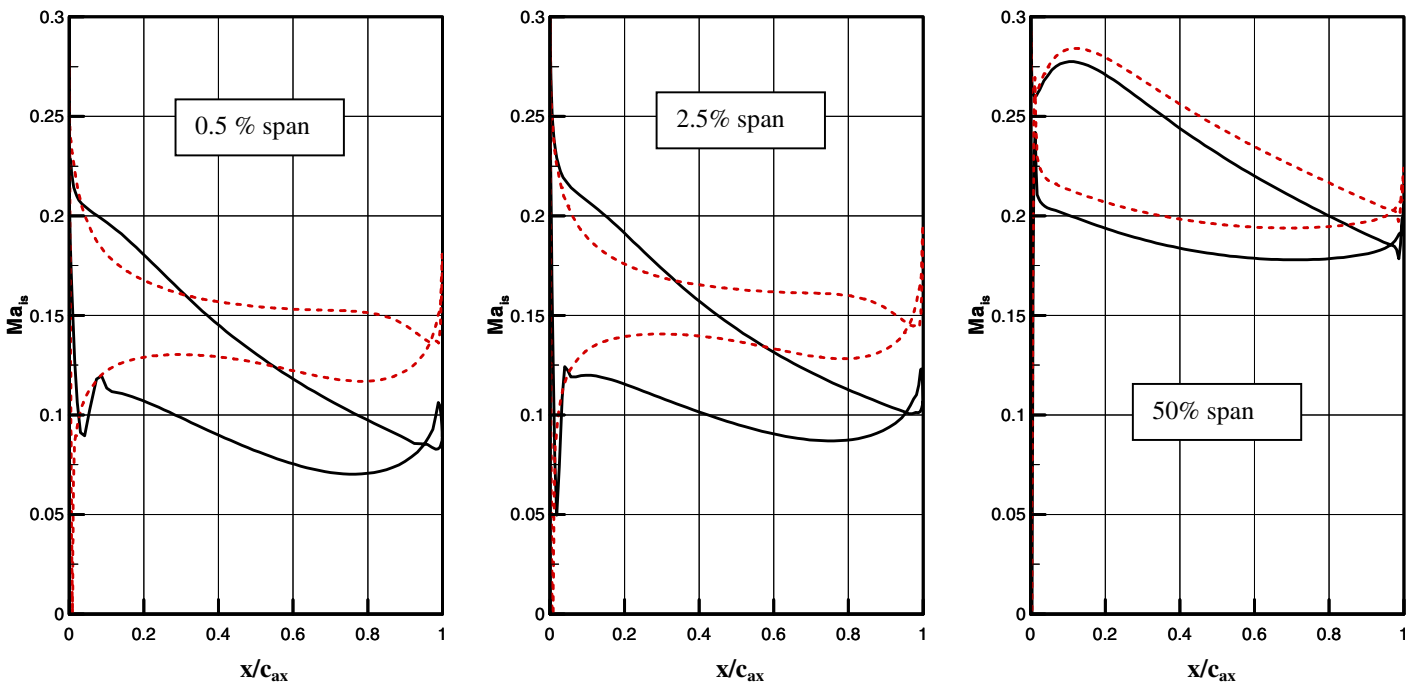


Fig. 14 Comparison of isentropic profile section Mach number distributions. Twisted boundary layer inlet profile sw15 fillet r8 (full line) vs. datum configuration (dashed, red line) at stations near endwall (0.5% span), at half fillet height (2.5% span) and in 2D flow (50%span).

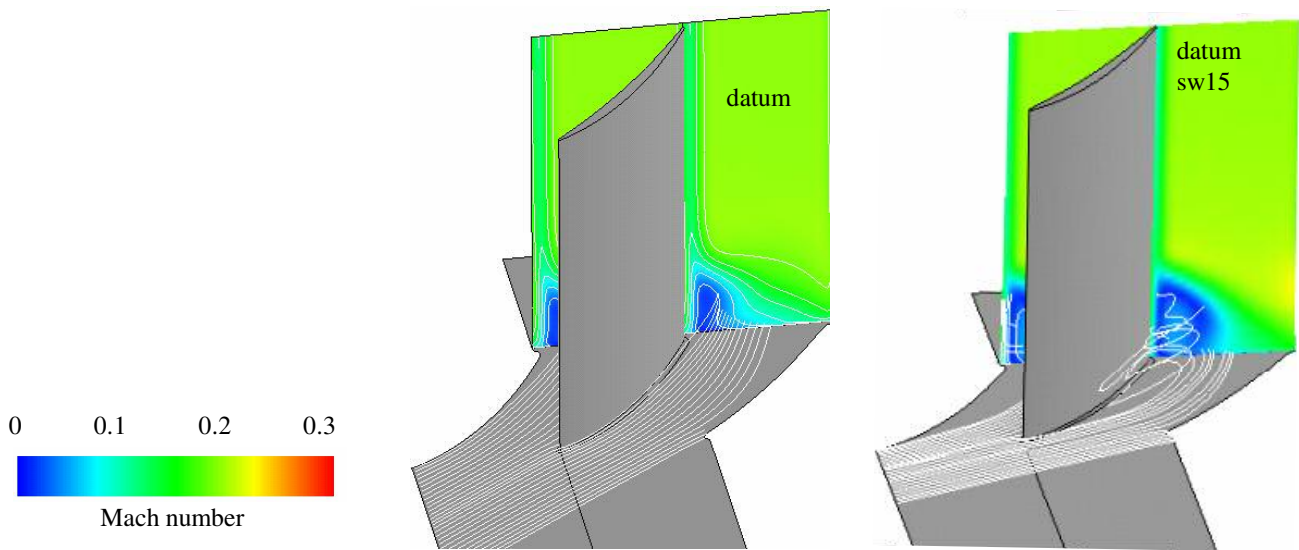


Fig. 15: Streamlines and Mach number contours in a plane close to the cascade exit.  
Datum cascade with constant inlet swirl (left side), onset of corner stall  
Datum cascade with about 15 deg twisted inlet boundary layer profile, fully stalled

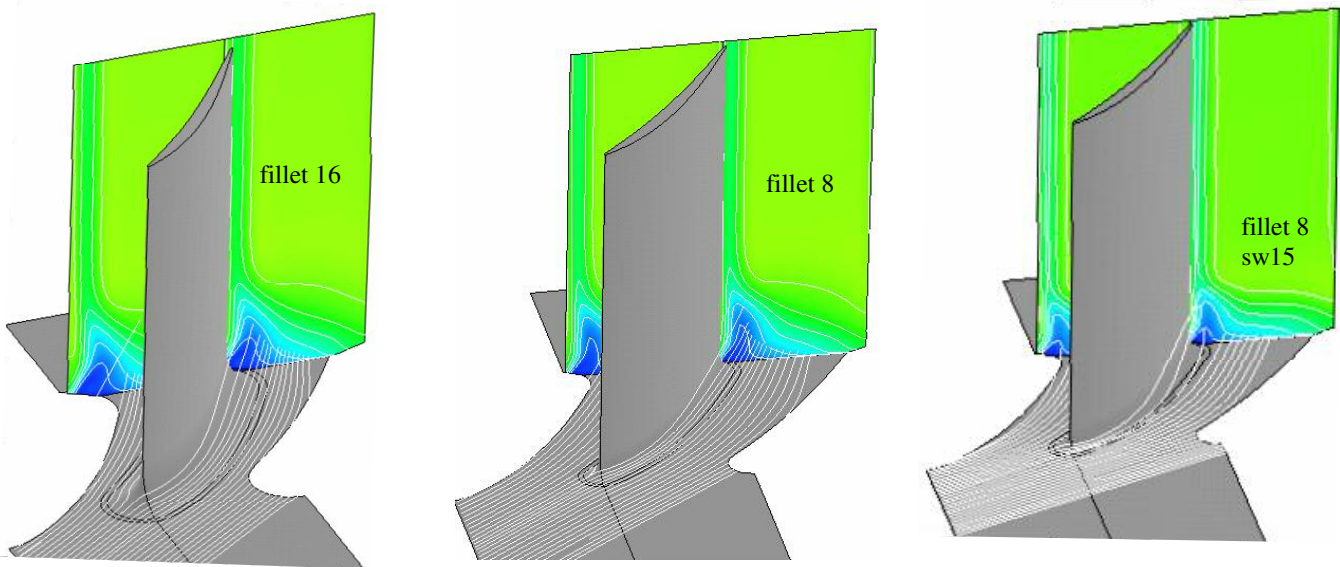


Fig. 16: Streamlines and Mach number contours in a plane close to the cascade exit.  
Fillet 16 with constant inlet swirl (left side), delayed onset of corner stall  
Fillet 8 with constant inlet swirl (mid), delayed onset of corner stall  
Fillet 8 with about 15 deg twisted inlet boundary layer profile (right side), reduced corner stall

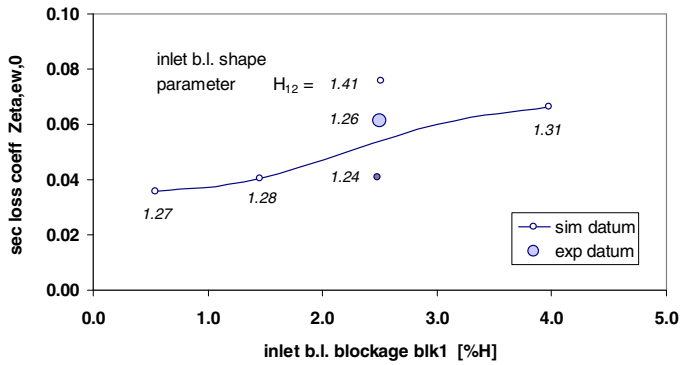


Fig. 17: Impact of inlet boundary layer blockage on total net endwall loss coefficient. Datum cascade

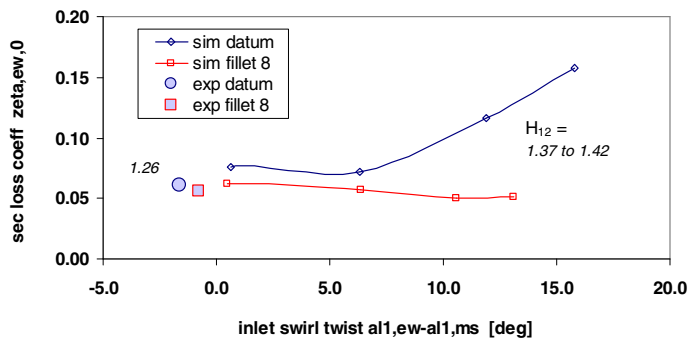


Fig. 18: Impact of inlet boundary layer twist on total net endwall loss coefficient. Datum cascade

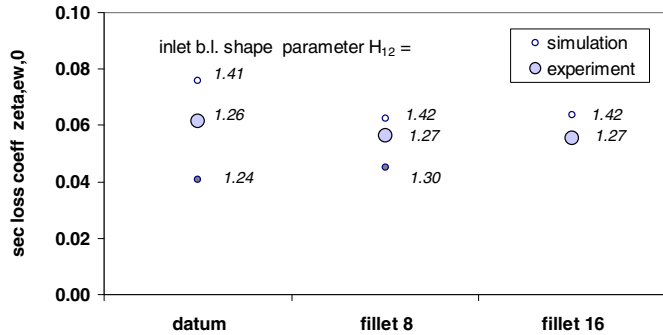


Fig. 19: Comparison of measured and predicted total net endwall loss coefficients for the cascade configurations investigated.

Mach number level and less diffusion from blockage generated by a corner separation developing at this incidence. At 50% span the Mach number distributions are nearly identical. This indicates the inlet conditions between the mid section (100% span) and the endwall to be nearly independent of the endwall flow. Note a stagnation point not to exist for spanwise stations below 3% span (approximately the half fillet

radius wall distance and about 60 deg inclination relative to the endwall) in Fig. 13.

For the simulations with the highest inlet boundary layer twist sw15 the datum cascade is no longer able to withstand the high incidences at the endwall and a complete separation is visible in Fig. 14. The pronounced variation in profile section Mach numbers at 50% span indicates a strong interaction with the endwall flow to occur. For fillet 8 the higher inlet flow angles at the endwall generate an increase in turning and diffusion. At 50% span fillet 8 Mach number distributions with and without swirl distortion again compare quite nicely.

**Exit Flow Field:** An explanation for the high diffusion capability of the fillet 8 configuration is found from the streamline patterns and Mach number plots close to the cascade exit plane. The datum cascade in Fig. 15, left side clearly shows a corner stall. The dead air region on the suction surface stems not only from corner stall but in addition from convective transport of endwall boundary layer material by secondary flow, the so-called passage vortex. For the datum vane and 15 deg swirl distortion the corner stall already starts at the leading edge, see Fig. 15, right side, and the cascade endwall region is demonstrated to be fully separated.

The situation changes completely for the fillet 8 case shown in Fig. 16, mid, where a much smaller dead air region is found on the suction surface. If now an engine like swirl distortion sw15 is introduced, the cross flow is blocked, Fig. 16, right side. Even for higher turnings at the endwall a more homogeneous exit flow field is obtained, which allows for the increased diffusion levels already observed in the Mach number distributions of Fig. 14.

Large fillet 16 results are finally presented in Fig. 16, left side. A similar flow pattern is obtained as for the smaller fillet. However, the increased bluntness promotes the formation of a dead air region in the vicinity of the trailing edge endwall junction

### Net Endwall loss coefficients

A comparison of net endwall loss coefficients, see eq. (2), for simulations for varying inlet boundary layer thickness is made in Fig. 17. The curve shows a tendency for increasing losses with inlet boundary layer displacement thickness and it flattens, when fully separated flow occurs at highest inlet displacement thickness. A considerable impact of the shape factor  $H_{12}$  is found.

The inlet swirl study was made to simulate engine like distorted swirl profiles in the cascade. A small reduction in endwall loss is found for 5 degree swirl distortion sw5 for both the fillet 8 and the datum configuration in Fig. 18. For higher endwall swirl twists of about 12 deg a steep increase in loss is predicted by the simulation only for the datum cascade, while the fillet benefits from the reduced cross-flow already discussed in Fig 14, right side.

A comparison of measured and predicted total net endwall loss coefficients in Fig. 19 gives reasonable agreement for datum and fillet configurations. The somewhat lower losses predicted from the simulations with the inlet boundary layer displacement thickness and shape factor  $H_{12}$  close to the experiment can partly be explained by the fact that in experiment at midspan laminar boundary layer transition occurred, while the simulation were run in the fully turbulent mode.

## CONCLUSIONS

To investigate the influence of a fillet on secondary flow, a 2D compressor cascade was designed at MTU Aero Engines and investigated experimentally at Dresden University of Technology. The simulations with a  $k-\omega$  turbulence model showed good agreement with experimental results at stalled conditions in principle. Total net endwall loss levels for 2 fillet configurations were predicted by the 3D Navier-Stokes code in close agreement to the measurements.

On the basis of steady simulations the magnitude of the inlet boundary layer thickness, its shape parameter and a twist in inlet swirl was demonstrated to significantly impact the endwall losses. For engine-like inlet boundary layer twist distortions of about 15 degrees, the datum cascade was fully stalled. At the same inlet conditions prescribed far upstream, the fillet configuration showed attached flow at the leading edge. The high incidence swirl entered the cascade passage, unimpeded and reduced the secondary cross flow, resulting in a reduction of the endwall boundary layer low energy material convection on the suction surface. By that, the corner stall was delayed and a higher diffusion ratio together with lower endwall losses is made possible.

However, for large fillet configurations no precisely defined exit flow condition (*Kutta*-condition) exists. Here advanced modeling with an unsteady solver and a multi-stage approach may help to further improve the prediction of stall in a compressor stage.

## ACKNOWLEDGMENTS

Most of the work has been performed as part of AG TURBO program and has been supported financially by the Ministry of Economic Affairs and Employment under contract No. 0327060E.

## REFERENCES

- [1] Vo, H.D., Tan, C.S., Greitzer, E.M., 2005, “ *Criteria for Spike Initiated Stall* ”, ASME-Paper GT2005-68374.
- [2] Deppe, A., Saathoff, A., Stark, U., 2005, “ Spike-Type Stall Inception in Axial Compressors ”, Proceedings of the 6<sup>th</sup> European Conference on Turbomachinery, Lille, France, March 2005.
- [3] Stringham, G.D., Cassem, B.N., Prince, T.C., Yeung, P.F., 1998, “Design and development of a nine stage axial flow compressor for industrial gas turbines“, ASME-Paper 98-GT-140.
- [4] Hoeger, M., Sievers, N., Lawrenz, M., 2001, “On the performance of compressor blades with contoured end-walls“, Proceedings of the 4<sup>th</sup> European Conf. On Turbomach., Florence, pp. 711-720.
- [5] Sauer, H., Müller, R. Vogeler, K., 2000, “Reduction of Secondary Flow Losses in Turbine Cascades by Leading Edge Modifications at the Endwall“, ASME-Paper 2000-GT-473.
- [6] Shih, T. I-P., Lin, Y.-L., 2003, Controlling Secondary Flow Structure by Leading-Edge Airfoil Fillet and Inlet Swirl to Reduce Aerodynamic Loss and Surface Heat Transfer, Transactions of the ASME, Vol. 125, Jan. 2003, pp. 48-56.
- [7] Sauer, H., Müller, R. Vogeler, K., 2003, “Influencing the Secondary Losses in Compressor Cascades by a Leading Edge Bulb Modification at the Endwall“, ASME-Paper No. 2000-GT-473.
- [8] Debruge, L.L., 1980, “The Aerodynamic Significance of Fillet Geometry in Turbocompressor Blade Rows ”, ASME J. of Engineering for Power, Vol.102, pp. 984-993.
- [9] Curlett, B.P., 1991, “The aerodynamic effect of fillet radius in a low speed compressor cascade”, National Aeronautics and Space Administration, Lewis Research Center, USA, NASA-TM-105347.
- [10] Breugelmans, F.A.E., 1999, “Experimental Investigation of Sweep and Dihedral in Compressors”, Von Karman Institute for Fluid Dynamics, Lecture Series 1999-02 on Turbomachinery Blade Design Systems.
- [11] Hoeger, M., Schmidt-Eisenlohr, U., Gomez, S., Müller, R., Sauer, H., 2002, “ Numerical Simulation of the Influence of a Bulb and a Fillet on the Secondary Flow in a Compressor Cascade“, TASK Quarterly 6 No. 1 (2002) pp. 25-57.
- [12] Klein, A., 1966, “Untersuchungen über den Einfluß der Zuströmungsgrenzschicht auf die Sekundärströmungen in den Beschaukelungen von Axialturbinen“, Forschung im Ingenieurwesen, Bd. 32 (1966) Nr. 6, pp. 175-188.
- [13] Sauer, H., Müller, R. Vogeler, K., Hoeger, M., 2004, “Influencing the Secondary Losses in Compressor Cascades by a Leading Edge Bulb Modification at the Endwall“, ASME-Paper No. 2004-GT-473.
- [14] K. Vogeler, R. Müller, 2005, “Fortschritt durch skalierte Niedergeschwindigkeitsversuche” 10 Jahre Versuchsbetrieb am Niedergeschwindigkeits-Axialverdichter der TU Dresden. Tagungsband zur 21. Strömungstechnischen Tagung, 2005, Der Andere Verlag, Tönning, Lübeck und Marburg. ISBN 3-89959-354-5.
- [15] Fritsch, G., Hoeger, M., Blaha, C., Bauer, D., 1997b, “Viscous 3D Compressor Simulation on Parallel Architectures”, AIAA Paper 97-2876.